Molybdenum Ditelluride Rendered into an Efficient and Stable Electrocatalyst for the Hydrogen Evolution Reaction by Polymorphic Control

Jessica C. McGlynn, Irene Cascallana-Matías, James P. Fraser, Isolda Roger, James McAllister, Haralampos N. Miras, Mark D. Symes,* and Alexey Y. Ganin*[a]

The electrocatalytic hydrogen evolution reaction (HER) is of central importance for the production of H_2 from sustainable sources. Currently, Pt is the best electrocatalyst for this transformation, but other materials based on less-precious elements are now attracting increased attention. Of these alternatives, the molybdenum chalcogenides show particular promise. MoS_2 has been explored extensively in this regard, which has highlighted the important role of polymorphism for catalytic activity. However, the conversion into an active polymorph is complex, and the stability of the catalyst under electrochemical conditions is poor. In contrast, $MoTe_2$ has been barely studied as an electrocatalyst for the HER. Herein, we isolate the semiconducting and metallic polymorphs of $MoTe_2$ using an easy solid-state route and show that interconversion between the two polymorphs of $MoTe_2$ can be achieved without a change in morphology by a simple temperature-annealing protocol. Although the semiconducting form is a rather poor electrocatalyst for the HER, the metallic 1T′-$MoTe_2$ polymorph is an efficient and stable electrocatalyst for the HER in 1 M H_2SO_4. Even in the bulk form, it achieved a low overpotential with a Tafel slope of (78 ± 4) mV dec^{-1} and full Faradaic efficiency. These findings highlight the importance of polymorphic control in the development of HER catalysts and suggest an efficient route for the discovery of new and improved electrocatalysts.

Introduction

Direct solar-to-hydrogen conversion using photoelectrochemical water splitting is an attractive approach to concentrate the power of incident sunlight into high-density energy storage.[1–4] The choice of electrocatalyst is critical as it will affect the efficiency, lifetime, and cost of the water-splitting apparatus.[5,6] Of the known electrocatalysts for the hydrogen evolution reaction (HER), noble metals are the best in terms of the maximum current densities that can be achieved at low overpotentials.[7,8] However, realistic current densities that might be attained in a typical photoelectrochemical water splitting system are on the order of 10 mA cm^{-2} (for both "direct" and "indirect" approaches) on account of the rather diffuse nature of sunlight (typically, a value of 1 kW m^{-2} is taken to be equivalent to "1 Sun").[2,3] These low current densities mean that electrodes of a very large surface area are needed to produce hydrogen at useful rates. Hence, expensive and scarce noble elements (Re, Ru, Os, Rh, Ir, Pd, Pt, Ag, and Au) would be rather impractical choices as electrocatalysts for solar-to-hydrogen devices. For non-noble metal electrocatalysts, much research has been performed on the sulfides of molybdenum, a promising class of catalysts for the evolution of hydrogen in acidic media. Experimental and computational studies have shown that the catalytic activity of the naturally occurring semiconducting hexagonal molybdenite (2H-MoS_2) phase is directly proportional to the edge length of the crystals but only weakly correlated to their basal planes.[9–11] This is in agreement with density functional theory (DFT) calculations, which indicate that only the edges of MoS_2 nanoparticles have a suitable site-dependent Gibbs free energy of hydrogen adsorption ($\Delta G_H = 0.08$ eV), whereas for the basal planes this value is as high as 2 eV.[12,13] A ΔG_H close to zero is favorable and indicates that hydrogen adsorption is neither too weak nor too strong, and this value correlates with exchange current densities that are a good approximation for HER activity. Site engineering by nanostructuring is required to achieve a high density of edge sites to overcome the limitations of the naturally occurring semiconducting hexagonal molybdenite (2H-MoS_2) phase, which is a remarkably inactive electrocatalyst in the bulk form.[14–19] However, nanostructuring tends to impair the long-term stability of the electrocatalyst, which reduces the operational

[a] J. C. McGlynn, Dr. I. Cascallana-Matías, J. P. Fraser, Dr. I. Roger, J. McAllister, Dr. H. N. Miras, Dr. M. D. Symes, Dr. A. Y. Ganin
School of Chemistry, WestCHEM
University of Glasgow
Glasgow (UK)
Fax: (+44) 141 330 4888
E-mail:
E-mail: mark.symes@glasgow.ac.uk
alexey.ganin@glasgow.ac.uk

Supporting information and the ORCID identification number(s) for the author(s) of this article can be found under: https://doi.org/10.1002/ente.201700489.

lifetime significantly.[3] Hence, the quest for materials that are electrocatalytically active in bulk form is important for future applications.

In this context, the exfoliation and restacking of Li-intercalated 2H-MoS_2 affords a metastable 1T-MoS_2 polymorph that is a highly efficient electrocatalyst in the bulk form.[20] Impressive Tafel slopes of 40 mV dec^{-1} have been reported for this polymorph, which does not occur naturally, that are only marginally worse than the slope of 30 mV dec^{-1} achieved for Pt.[21,22] The improved performance was attributed to a structural change in the coordination environment of Mo by S from trigonal prismatic (in the thermodynamically favored 2H-MoS_2 form) to a distorted octahedral coordination in the 1T phase. This structural transformation is accompanied by the appearance of metallic conductivity in 1T-MoS_2. The change in electronic properties leads to a dramatic reduction in ΔG_H, which in turn makes 1T-MoS_2 a highly efficient electrocatalyst even in the bulk form.[13,21] However, the low thermodynamic stability and complexity of the experimental preparation of the 1T phase remains a significant challenge. Furthermore, a careful evaluation of the Raman spectroscopy and powder X-ray diffraction (PXRD) data showed the presence of a 2H-MoS_2 phase impurity in line with earlier work by Kanatzidis et al.,[20] and it remains very challenging to isolate the 1T phase as a single-phase product.[20–22] Moreover, long-term stability experiments indicated the reverse transformation back to the more thermodynamically stable and inactive 2H phase.[22]

However, in the less prominent Mo–Te system, which has received little attention from electrochemistry researchers to date, a switch between the semiconducting 2H-$MoTe_2$ phase and the metallic 1T′-$MoTe_2$ phase with edge-distorted octahedral arrangements is achieved merely by altering the synthesis temperature.[23,24] Herein, we exploit this facile route to 1T′-$MoTe_2$ and demonstrate that even in the bulk form it can act as an efficient and stable electrocatalyst for the HER in 1 M H_2SO_4. In particular, we demonstrate that 1T′-$MoTe_2$ can achieve current densities of 10 mA cm^{-2} at 340 mV overpotential with a Tafel slope of 78 mV dec^{-1} and full Faradaic efficiency for hydrogen production. When tested under the same conditions, the electrochemical performance of semiconducting 2H-$MoTe_2$ was inferior, which suggests that polymorphic control is key for the development of future efficient electrocatalysts.

Results and Discussion

Reactions between Mo and Te powders in sealed ampoules at elevated temperatures yield black homogeneous products with a metallic luster. We used PXRD to identify the product of quenching into iced water from 900 °C as single-phase 1T′-$MoTe_2$ with no elemental Mo or Te present within the sample (Figure 1). The pattern matches that reported by Brown for a monoclinic, high-temperature $MoTe_2$ phase.[25] Synchrotron XRD (I22) data were collected for 1T′-$MoTe_2$ at ambient temperature and confirmed the single-phase nature of the sample. LeBail refinement of the PXRD data

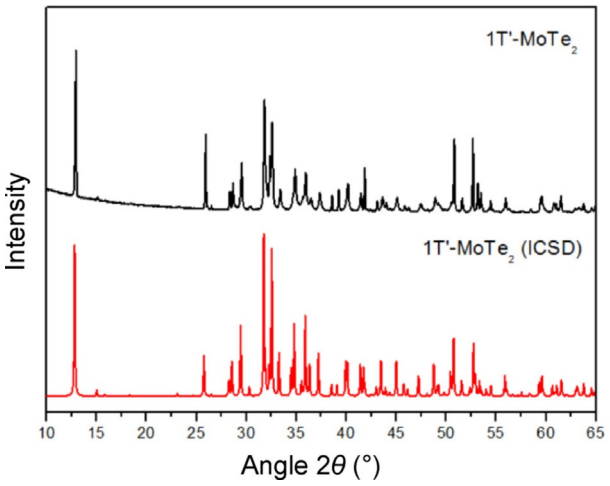

Figure 1. Powder X-ray diffraction pattern of 1T′-$MoTe_2$ (top) and a simulated diffraction pattern from the ICSD database (bottom).[25]

was performed using a structural model reported previously,[25] and the unit cell was indexed to a monoclinic unit cell of dimensions: $a = 6.32985(6)$ Å; $b = 3.47827(2)$ Å; $c = 13.8178(2)$ Å, $\beta = 93.838(1)°$ (see Experimental Section and Figure S1, Supporting Information, for details).

Subsequent annealing of the monoclinic 1T′-$MoTe_2$phase powders at 700 °C for 24 h gives a diffraction pattern that matches that simulated for hexagonal 2H-$MoTe_2$ (Figure S2, Supporting Information). Raman spectroscopy was employed to further confirm the phase purity of the materials. The spectrum of 1T′-$MoTe_2$ is shown in Figure 2, in which the major peak corresponds to the B_g vibrational mode.[26,27] Notably, there are no peaks at approximately $\tilde{\nu} = 750$ and 800 cm^{-1} that correspond to MoO_2 and MoO_3, which confirms that the sample contained a single-phase polymorph.[28] We also used Raman spectroscopy to show that the annealing of 1T′-$MoTe_2$ at 700 °C leads to polymorphic conversion

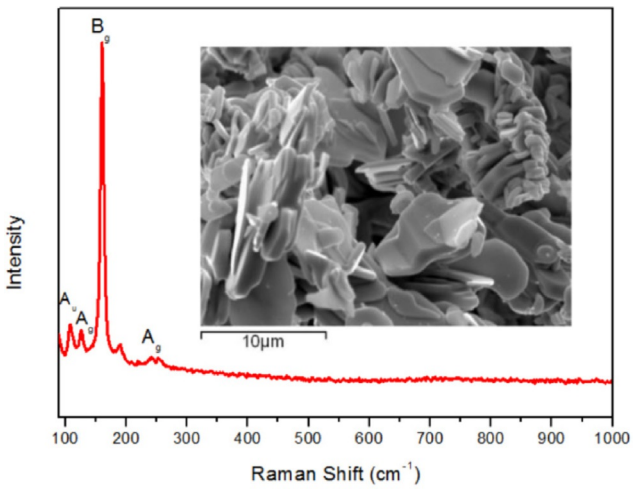

Figure 2. Wide-range Raman spectrum of 1T′-$MoTe_2$ with four major vibrational modes highlighted. The inset shows particle morphology from SEM images.

into phase-pure 2H-$MoTe_2$ (Figure S3, Supporting Information).

We used SEM to reveal that metallic 1T′-$MoTe_2$ consists of platelike microcrystals (Figure 2, inset). The morphology was preserved upon polymorphic transformation to the semiconducting 2H-$MoTe_2$ material (Figure S4, Supporting Information). The microcrystalline, platelike morphology of the $MoTe_2$ products clearly shows that both materials are bulk and that basal planes rather than edge sites are available for the electrocatalytic reaction. Furthermore, the identical particle morphology of the two distinct phases also reiterates that the polymorphic transition is the only difference between the two investigated catalysts.

Additionally, energy-dispersive X-ray spectroscopy (EDX) was performed to confirm the elemental composition of both phases, and the weight and atomic compositions were averaged over six areas for each sample. The stoichiometries of 1T′-$MoTe_2$ and 2H-$MoTe_2$ were determined to be $Mo_{1.06(5)}Te_{1.94(5)}$ and $Mo_{1.00(9)}Te_{2.00(9)}$, respectively. These compositions correspond well with the elemental analysis evaluated using inductively coupled plasma optical emission spectroscopy (ICP-OES), which gave stoichiometric compositions of $Mo_{1.00}Te_{2.01(3)}$ and $Mo_{1.00}Te_{2.03(7)}$ for 1T′-$MoTe_2$ and 2H-$MoTe_2$, respectively. Evidently, the elemental compositions of both the semiconducting and metallic phases are identical within experimental error. Therefore, by a simple change in reaction temperature, both phases can be formed without the need for complex chemical exfoliation by Li intercalation as required for MoS_2, which thereby ensures that the only difference between the phases is their coordination geometry.

A comparison of the current densities achieved using both 1T′-$MoTe_2$ and 2H-$MoTe_2$ products, which were prepared for electrochemical testing by depositing the catalysts onto the surface of a glassy carbon electrode, is shown in Figure 3.[29] In addition, the overpotentials required by each catalyst to reach a current density of $j = 10\ mA\,cm^{-2}$ are summarized in Table S1 (Supporting Information).

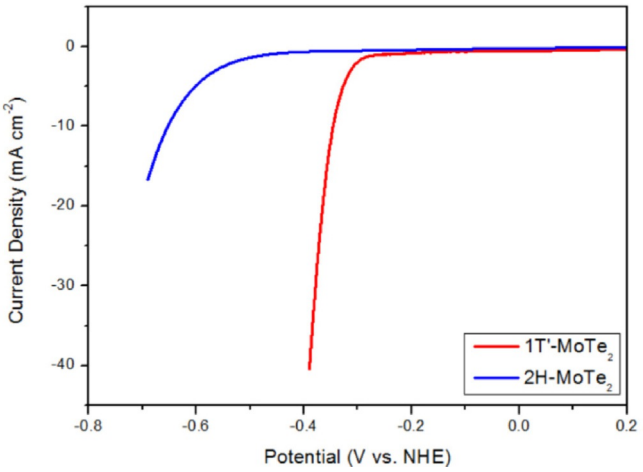

Figure 3. Comparison of the current densities achieved by each catalyst in 1 M H_2SO_4 electrolyte. Catalysts were prepared on a glassy carbon working electrode as described in the Experimental Section. A 3 M Ag/AgCl reference electrode and Pt wire counter electrode were used. Curves were obtained using linear sweep voltammetry at a scan rate of 2 $mV\,s^{-1}$.

Upon initial inspection of the overpotentials, the semiconducting 2H-$MoTe_2$ requires significantly greater cathodic potentials to reach a given current density than metallic 1T′-$MoTe_2$. Consequently, the 1T′-$MoTe_2$ phase requires less energy to reduce protons to hydrogen than the 2H-$MoTe_2$ phase, which is in line with recent computational experiments.[24] With a decrease in the overpotential of approximately 310 mV (at $10\ mA\,cm^{-2}$), it is apparent that upon the transition from the hexagonal to monoclinic structure, the activity for the HER increased.

However, to determine if the reaction kinetics are also enhanced and, therefore, if the 1T′-$MoTe_2$ phase is indeed catalytically more active than the 2H-$MoTe_2$ phase, the Tafel slopes were measured. The Tafel plots of the investigated catalysts are shown in Figure 4, and the corresponding Tafel slopes, which determine the kinetics of the reaction, are summarized in Table S1 (Supporting Information). Ideally, an efficient HER catalyst reaches the highest possible current density at the lowest possible overpotential. For example, Pt possesses the smallest reported Tafel slope for the HER of $30\ mV\,dec^{-1}$. This is due to the exceptionally efficient adsorption of hydrogen onto the Pt surface. The reaction mechanism can be interpreted from the Tafel slope, and hydrogen production on Pt is known to proceed by the Volmer–Tafel mechanism.[30] In the case of 2H-$MoTe_2$, a Tafel slope of $(159 \pm 6)\ mV\,dec^{-1}$ was obtained, which indicates that the kinetics of the HER are extremely sluggish. This is perfectly in line with earlier research that supports inefficient hydrogen adsorption on bulk 2H-MoS_2, most likely because of the vast quantity of basal plane sites rather than the catalytically active edge sites in the bulk material.[13]

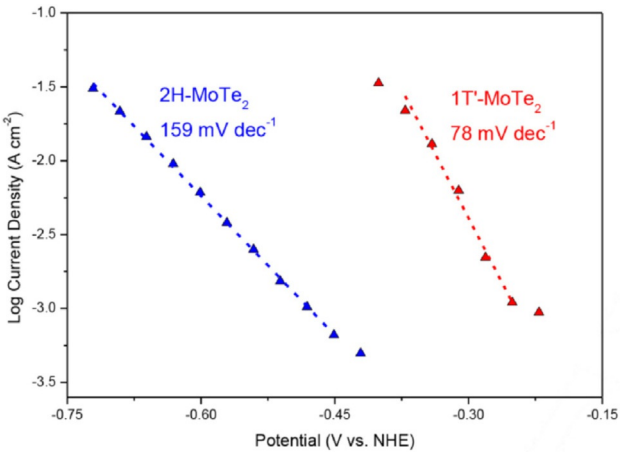

Figure 4. Tafel plots of the two polymorphs in 1 M H_2SO_4. Plots were obtained as per the conditions described in the Experimental Section, and the current density was recorded after each potential had been applied for 5 min. The dashed lines are provided as a guide to the eye. All current densities have been corrected for resistance.

Upon polymorphic conversion from 2H-$MoTe_2$ to 1T′-$MoTe_2$, the Tafel slope is halved. This lower Tafel slope of

(78 ± 4) mV dec^{-1} corresponds well with previous reports for 1T-MoS_2 that suggest that the adsorption of hydrogen on metallic active sites is much more efficient than on semiconducting sites.[21] As a result of the metallic character of the monoclinic 1T′-$MoTe_2$ phase, charge transfer is facilitated more easily. Thus, significantly higher current densities are achieved at overpotentials considerably lower than the semiconducting 2H-$MoTe_2$. Further, the turnover frequencies (TOFs) were calculated under the assumption that each individual atom in both materials was catalytically active (Supporting Information). As such, at $\eta = 340$ mV, TOFs of 0.102 and 0.010 s^{-1} atom^{-1} were obtained for 1T′-$MoTe_2$ and 2H-$MoTe_2$, respectively. These values are in line with the corresponding Tafel slopes and reiterate the greater efficiency of the metallic 1T′-$MoTe_2$ in comparison with the semiconducting phase.

In addition to Tafel slopes, electrochemical impedance spectroscopy (EIS) was used to elucidate the difference in charge transfer kinetics between the two phases of $MoTe_2$. The Nyquist plots that show the EIS on 2H-$MoTe_2$ and 1T′-$MoTe_2$ at a potential of −0.2 V (vs. the normal hydrogen electrode; NHE) are presented in Figure S5 (Supporting Information). The charge transfer resistances R_{CT} of 2H-$MoTe_2$ and 1T′-$MoTe_2$ can be extrapolated from the Nyquist plots and were determined to be 75 and 9 kΩ, respectively. This decrease in the charge transfer resistance is attributed to the conductive properties of metallic 1T′-$MoTe_2$. This allows for a much more efficient charge transfer as reported previously for metallic 1T-MoS_2 nanosheets, which therefore, results in an increased activity for the HER.[21,22] Thus, we can confirm that the phase transition from semiconducting to metallic $MoTe_2$ does indeed result in improved catalytic activity for the HER.

The electrochemical stability of 1T′-$MoTe_2$ was investigated using cyclic voltammetry (CV) by sweeping the applied potential continuously between 0.2 and −0.4 V (vs. NHE) for 1000 cycles. The electrochemical stability of 1T′-$MoTe_2$ is shown in Figure 5, and the overpotential was maintained at its original value of −0.34 V (for a current density of 10 mA cm^{-2}). No loss of catalytic activity is observed, which implies that the 1T′-$MoTe_2$ phase is a stable electrocatalyst for the HER. Similarly, bulk electrolysis was performed for 18 h and the overpotential was held at −0.34 V. During the first 5 h of electrolysis, a decrease in the current density was observed until the current stabilized at approximately 10 mA cm^{-2}, as expected at this applied potential (Figure S6, Supporting Information).

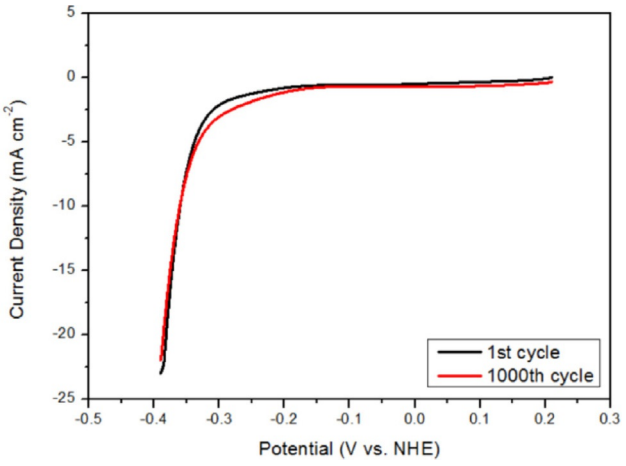

Figure 5. Stability test of 1T′-$MoTe_2$ in 1 M H_2SO_4 electrolyte obtained by the continuous sweeping of the applied potentials for 1000 cycles using cyclic voltammetry.

In the case of 2H-$MoTe_2$, the potential was swept continuously between 0.2 and −0.74 V (vs. NHE) for 1000 cycles (Figure S7, Supporting Information). Upon cycling, it is clear that, within experimental error, the overpotential of 2H-$MoTe_2$ remains constant. Therefore, the semiconducting 2H-$MoTe_2$ phase can be described as a stable catalyst for the HER, which is less efficient than the metallic phase because of the greater overpotential.

Raman spectroscopy was employed to observe any structural changes before and after the electrochemical measurements. Raman spectra of 1T′-$MoTe_2$ and 2H-$MoTe_2$ before and after the 1000 cycle CV scans are shown in Figure 6 and

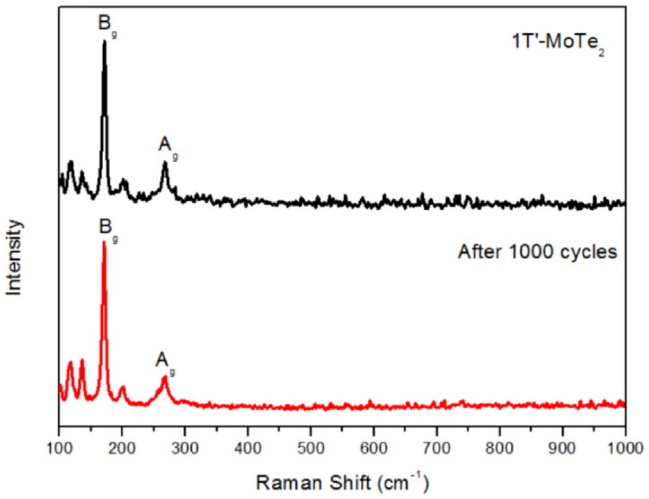

Figure 6. Comparison of the Raman spectra of 1T′-$MoTe_2$ obtained before and after stability tests.

Figure S8 (Supporting Information). Clearly, there are no detrimental structural changes with continuous CV cycling, that is, $MoTe_2$ does not decompose into MoO_3 or elemental Te. There is no evidence for the deposition of Ag on the electrode, which rules out Ag^+ leakage from the reference electrode as a cause for the activity observed.[31] Furthermore, there is no evidence for transformation into the 2H-$MoTe_2$ phase, unlike the behavior found earlier for MoS_2 polymorphs.[22] Therefore, the materials appear to be stable electrocatalysts for the HER.

Finally, we used gas chromatography (GC) to confirm that the reduction potential observed using linear sweep voltammetry (LSV) corresponds to the reduction of protons to hydrogen. As such, the Faradaic efficiency of the 1T′-$MoTe_2$

catalyst in 1 M H_2SO_4 was determined to be (95±8)%. A representative trace of the GC analysis of the headspace in an airtight cell is shown in Figure 7, which confirms the production of hydrogen using 1T′-$MoTe_2$ as the HER catalyst. In contrast, the Faradaic efficiency of 2H-$MoTe_2$ was determined to be (82±14)% (Figure S9, Supporting Information). As such, it is clear that although the semiconducting polymorph is able to evolve hydrogen, it requires much more energy and is less efficient than the metallic 1T′-$MoTe_2$.

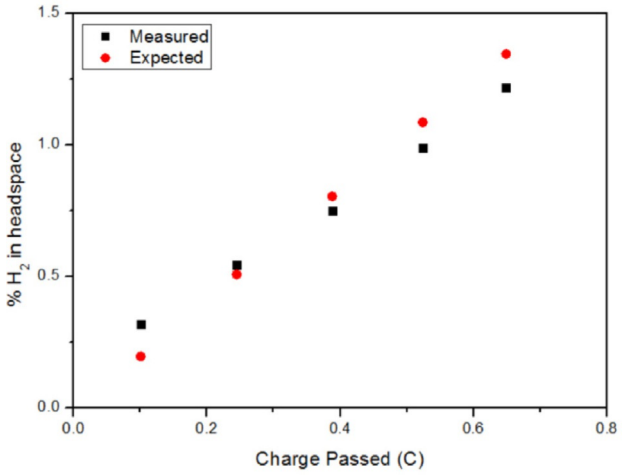

Figure 7. A representative trace of the gas chromatographic analysis of the single-cell headspace during the electrolysis of 1T′-$MoTe_2$ in which a constant current of −0.24 mA was applied in 1 M H_2SO_4. The expected proportion [%] of H_2 in the headspace was calculated from the charge passed, and the proportion [%] of H_2 measured experimentally was determined using gas chromatography. Black squares indicate actual measurements of the proportion of H_2 in the cell headspace determined using gas chromatography.

Conclusions

We have shown that both the metallic and semiconducting polymorphs of $MoTe_2$ can be isolated as single-phase products by a solid-state approach, which requires only a change in the synthesis temperature to induce the phase transition. This is in contrast to existing routes to induce a similar phase transition in MoS_2, which require much more elaborate methods. Upon the polymorphic transformation between 1T′-$MoTe_2$ and 2H-$MoTe_2$ the morphology is retained, which allowed us to investigate and compare the electrocatalytic activities of semiconducting and metallic polymorphs of $MoTe_2$ in the bulk form. We used electrochemical testing to show that metallic 1T′-$MoTe_2$ has superior catalytic activity towards the hydrogen evolution reaction in comparison with the semiconducting form. This is borne out by faster reaction kinetics, which we attribute to the decreased charge transfer resistance of the metallic phase. In contrast to nanostructured MoS_2 catalysts, bulk 1T′-$MoTe_2$ is stable after continuous cyclic voltammetry cycling and long-term electrolysis, and no structural transformation into 2H-$MoTe_2$ was observed. Thus, polymorphic control allows access to a highly efficient electrocatalyst in the bulk form, which therefore, presents a new approach for the future development of catalysts for the hydrogen evolution reaction.

Experimental Section

Synthesis

The metallic 1T′-$MoTe_2$ phase was prepared by the stoichiometric reaction of the individual elements. Mo (Sigma–Aldrich, 99.95%) and Te (Alfa Aesar, 99.999%) were sealed in a quartz tube under a vacuum pressure of 4.5×10^{-2} mbar and shaken carefully to homogenize the mixture. The synthesis of metallic 1T′-$MoTe_2$ involved heating the powders to 900 °C (heating rate 5 °C min^{-1}) for 19 h, followed by quenching in water at this temperature to form the phase-pure metallic material.[23] The synthesis of semiconducting 2H-$MoTe_2$ was adapted from a procedure reported by Jana et al., which consisted of heating the powders of 1T′-$MoTe_2$ to 700 °C at a heating rate of 5 °C min^{-1} and holding for 24 h before it was allowed to cool to room temperature naturally.[26]

Characterization

PXRD was used to determine the phase purity of the materials. The measurements were performed using a Panalytical Xpert-pro diffractometer with CuK_α radiation ($\lambda=1.54178$ Å) operated in Bragg–Brentano geometry. Synchrotron powder X-ray diffraction (SXRD) data were collected at ambient temperature from powder loaded into 0.3 mm capillaries using the ID22 beamline [$\lambda=0.3998490(1)$ Å] at the European Synchrotron Radiation Facility (ESRF). Before the powder was loaded, it was reground with glass powder to minimize the adsorption and preferred orientation. However, despite all efforts to eliminate the preferred orientation, it still had a significant impact as revealed by high intensity of the associated peaks. Therefore, only LeBail refinements of the SXRD were performed by using the GSAS/EXPGUI software package.[32] For further phase-purity analysis, Raman spectroscopy was performed using a Horiba Jobin–Yvon LabRam Raman HR800 operated with a $\lambda=514$ nm laser. To prevent the degradation of the sample, a 1% filter was used. An aperture size of 100 μm was applied.

Scanning electron microscopy (SEM) images were obtained by using a Phillips XL30 ESEM instrument coupled with an Oxford Instruments X-act spectrometer for EDX measurements. The EDX was calibrated using the INCA EDX software with Cu as the calibration standard. ICP-OES was performed using an Agilent 5100 calibrated to a range of known-concentration [ppm] solutions of Mo and Te.

Electrochemical measurements

The electrochemical performance was investigated using a CH Instruments CHI760D potentiostat with a three-electrode setup in 1 M H_2SO_4 electrolyte unless otherwise stated. We followed the procedure of Gao et al.[29] to prepare the catalysts as inks and deposited them onto a glassy carbon working electrode (surface area 0.071 cm^2). This involved the sonication of 1 mL water/ethanol (3:1), 80 μL Nafion, and 10 mg catalyst for 1–2 h. The resulting catalyst ink (30 μL) was then dropcast onto the surface of the glassy carbon electrode. Pt wire and 3 M Ag/AgCl were used as the counter and reference electrodes, respectively. The electrode

potentials were converted to the NHE scale by $E(\mathrm{NHE}) = E(\mathrm{Ag/AgCl}) + 0.209$ V, and the Ohmic resistances were compensated.

CV and bulk electrolysis were performed using a three-electrode setup in a single-compartment electrochemical cell with a scan rate of 0.1 $\mathrm{V\,s^{-1}}$. Similarly, LSV was performed using the same three-electrode setup under constant stirring at a scan rate of 2 $\mathrm{mV\,s^{-1}}$. Tafel plots were collected at fixed potentials in increments of 30 mV. Each potential was held for 5 min, after which the current density was recorded and the Tafel slope was calculated. The cell was kept under continuous stirring to remove any bubbles from the surface of the working electrode.

EIS was measured and Nyquist plots were obtained at frequencies between 200 kHz and 50 mHz. These measurements were performed using a Biologic SP-150 potentiostat using the same three-electrode setup as described previously.

GC was utilized to confirm that the measured currents corresponded to the reduction of protons to hydrogen using an Agilent GC 7890 A with a thermal conductivity detector. The GC system was calibrated using certified standards of hydrogen at various concentrations (vol%) in Ar (CK Gas Products Limited, UK) before use. Faradaic efficiency measurements were obtained using a single airtight cell after degassing under Ar. Galvanostatic electrolysis was performed using a two-electrode setup that consisted of a Pt counter electrode, and the catalyst was deposited on a glassy carbon working electrode as described above. Before we measured the Faradaic efficiency of the investigated catalyst, the experiment was performed using Pt as the working electrode to ensure that the cell was airtight. A constant current of −0.24 mA was applied in both cases. The headspace was sampled (25 μL) and injected directly into the GC at appropriate intervals. Faradaic efficiencies were then calculated as the ratio of expected H_2 (%) in the headspace (as calculated from the charge passed) to the H_2 (%) detected using GC.

Acknowledgements

We acknowledge the University of Glasgow and the EPSRC (grant numbers EP/K031732/1 and EP/P001653/1) for funding. M.D.S. thanks the Royal Society for a University Research Fellowship. We thank Mr. Jim Gallagher (University of Glasgow) for assistance with the SEM measurements and Prof. Leroy Cronin and the Glasgow Solar Fuels network (University of Glasgow) for the use of shared facilities.

Conflict of interest

The authors declare no conflict of interest.

Keywords: electrochemistry · hydrogen · molybdenum telluride · polymorphism · water splitting

[1] N. S. Lewis, D. G. Nocera, *Proc. Natl. Acad. Sci. USA* **2006**, *103*, 15729–15735.
[2] S. Y. Reece, J. A. Hamel, K. Sung, T. D. Jarvi, A. J. Esswein, J. J. H. Pijpers, D. G. Nocera, *Science* **2011**, *334*, 645–648.
[3] I. Roger, M. A. Shipman, M. D. Symes, *Nat. Rev. Chem.* **2017**, *1*, 0003.
[4] M. D. Symes, *Makara J. Sci.* **2016**, *20*, 155–159.
[5] N. Armaroli, V. Balzani, *Chem. Eur. J.* **2016**, *22*, 32–57.
[6] C. C. L. McCrory, S. Jung, I. M. Ferrer, S. M. Chatman, J. C. Peters, T. F. Jaramillo, *J. Am. Chem. Soc.* **2015**, *137*, 4347–4357.
[7] D. V. Esposito, S. T. Hunt, A. L. Stottlemyer, K. D. Dobson, B. E. McCandless, R. W. Birkmire, J. G. Chen, *Angew. Chem. Int. Ed.* **2010**, *49*, 9859–9862; *Angew. Chem.* **2010**, *122*, 10055–10058.
[8] J. K. Nørskov, T. Bligaard, A. Logadottir, J. R. Kitchin, J. G. Chen, S. Pandelov, U. Stimming, *J. Electrochem. Soc.* **2005**, *152*, J23–J26.
[9] B. Hinnemann, P. G. Moses, J. Bonde, K. P. Jørgensen, J. H. Nielsen, S. Horch, I. Chorkendorff, J. K. Nørskov, *J. Am. Chem. Soc.* **2005**, *127*, 5308–5309.
[10] T. F. Jaramillo, K. P. Jørgensen, J. Bonde, J. H. Nielsen, S. Horch, I. Chorkendorff, *Science* **2007**, *317*, 100–102.
[11] J. Greeley, T. F. Jaramillo, J. Bonde, I. Chorkendorff, J. K. Nørskov, *Nat. Mater.* **2006**, *5*, 909–913.
[12] W. Jaegermann, H. Tributsch, *Prog. Surf. Sci.* **1988**, *29*, 1–167.
[13] C. Tsai, K. Chan, J. K. Nørskov, F. Abild-Pedersen, *Surf. Sci.* **2015**, *640*, 133–140.
[14] J. Kibsgaard, Z. Chen, B. N. Reinecke, T. F. Jaramillo, *Nat. Mater.* **2012**, *11*, 963–969.
[15] D. Merki, S. Fierro, H. Vrubel, X. Hu, *Chem. Sci.* **2011**, *2*, 1262–1267.
[16] X. Zou, Y. Zhang, *Chem. Soc. Rev.* **2015**, *44*, 5148–5180.
[17] I. Roger, R. Moca, H. N. Miras, K. G. Crawford, D. A. J. Moran, A. Y. Ganin, M. D. Symes, *J. Mater. Chem. A* **2017**, *5*, 1472–1480.
[18] H. Li, C. Tsai, A. L. Koh, L. Cai, A. W. Contryman, A. H. Fragapane, J. Zhao, H. S. Han, H. C. Manoharan, F. Abild-Pedersen, J. K. Nørskov, X. Zheng, *Nat. Mater.* **2016**, *15*, 48–53.
[19] D. Voiry, J. Yang, M. Chhowalla, *Adv. Mater.* **2016**, *28*, 6197–6206.
[20] J. Heising, M. G. Kanatzidis, *J. Am. Chem. Soc.* **1999**, *121*, 11720–11732.
[21] D. Voiry, M. Salehi, R. Silva, T. Fujita, M. Chen, T. Asefa, V. B. Shenoy, G. Eda, M. Chhowalla, *Nano Lett.* **2013**, *13*, 6222–6227.
[22] M. A. Lukowski, A. S. Daniel, F. Meng, A. Forticaux, L. Li, S. Jin, *J. Am. Chem. Soc.* **2013**, *135*, 10274–10277.
[23] M. B. Vellinga, R. de Jonge, C. Haas, *J. Solid State Chem.* **1970**, *2*, 299–302.
[24] J. Seok, J.-H. Lee, S. Cho, B. Ji, H. W. Kim, M. Kwon, D. Kim, Y.-M. Kim, S. H. Oh, S. W. Kim, Y. H. Lee, Y.-W. Son, H. Yang, *2D Mater.* **2017**, *4*, 025061.
[25] B. E. Brown, *Acta Crystallogr.* **1966**, *20*, 268–274.
[26] M. K. Jana, A. Singh, A. Sampath, C. N. R. Rao, U. V. Waghmare, *Z. Anorg. Allg. Chem.* **2016**, *642*, 1386–1396.
[27] D. H. Keum, S. Cho, J. H. Kim, D.-H. Choe, H.-J. Sung, M. Kan, H. Kang, J.-Y. Hwang, S. W. Kim, H. Yang, K. J. Chang, Y. H. Lee, *Nat. Phys.* **2015**, *11*, 482–486.
[28] A. S. Pine, G. Dresselhaus, *Phys. Rev. B* **1971**, *4*, 356–371.
[29] S. Gao, Y. Lin, X. Jiao, Y. Sun, Q. Luo, W. Zhang, D. Li, J. Yang, Y. Xie, *Nature* **2016**, *529*, 68–71.
[30] N. M. Marković, B. N. Grgur, P. N. Ross, *J. Phys. Chem. B* **1997**, *101*, 5405–5413.
[31] I. Roger, M. D. Symes, *ACS Appl. Mater. Interfaces* **2017**, *9*, 472–478.
[32] B. H. Toby, *J. Appl. Crystallogr.* **2001**, *34*, 210–213.

Manuscript received: July 19, 2017
Accepted manuscript online: July 19, 2017
Version of record online: September 21, 2017

